EUROPEAN COOPERATION
IN THE FIELD OF SCIENTIFIC
AND TECHNICAL RESEARCH

EURO-COST

SOURCE: Centre for Communications Research,
University of Bristol,
United Kingdom.

COST 273 TD(05)075
Bologna, Italy
2005/January/19-21

Outdoor Hotspot Dynamic Double-Directional Channel Measurements and Characterisations at 5 GHz*

* Paper initially presented at 7th Wireless Personal Multimedia Communications (WPMC) Conference, Italy, 12-15 September 2004

C. M. Tan, S. E. Foo, M. A. Beach, and A. R. Nix
Centre for Communications Research
Merchant Venturers Building
University of Bristol
Bristol BS8 1UB, UK.
Phone: + 44 117 954 5190
Fax: + 44 117 954 5206
Email: M.A.Beach@Bris.ac.uk

Outdoor Hotspot Dynamic Double-Directional Channel Measurements and Characterisations at 5 GHz

C. M. Tan, S. E. Foo, M. A. Beach, and A. R. Nix

Centre for Communications Research
Department of Electrical and Electronic Engineering
University of Bristol
Bristol BS8 1UB, UK.
Email: Chor.Min.Tan@bristol.ac.uk

***Abstract*— This paper describes samples of analysed results obtained from a high-resolution dynamic double-directional channel sounding campaign conducted in a hotspot courtyard environment. Post-processed results indicate that significant amount of multipath components (MPCs) concentrated along the axis where both transmitter (Tx) and receiver (Rx) faced each other. The global distributions of directional parameters at both sides were found to be uniformly distributed, with a peak exhibiting Laplacian characteristics around directional region where both terminals faced each other. Further, the capacity of multiple-input multiple-output (MIMO) channel has been evaluated based on reconstructed channel responses from knowledge of multipath parameters, and was found to provide excellent match with capacity computed from real measurement data.**

I. Introduction

Recall that the classical analysis of radio channels normally involves wideband characterisations only, whereby the power delay profile (PDP) and Doppler spectrum of the channels provide most information of interest for existing wireless technologies. However, following an increased interest in exploiting spatial domain properties for new communication technologies, e.g. smart antennas technique based on single-input multiple-output (SIMO) configuration [1][2], it is therefore necessary to perform joint spatial-temporal-frequency analysis for future research in order to facilitate a deeper understanding in the spatial domain. From physical propagation channel point of view and as far as channel characterisation and modelling involving spatial domain is concerned [3], this usually involves estimation of the directional parameter at one end of the link, e.g. direction of arrival (DoA) or direction of departure (DoD).

In addition, following the increased importance in exploiting MIMO architectures in order to gain spectral efficiency and throughput enhancement, it is also necessary to obtain a thorough understanding on spatial properties of MIMO channels. While single-directional information is considered sufficient for SIMO systems employing beamforming and smart antennas techniques, it is insufficient to support proper investigation and analysis of the MIMO channels. Further, no report can be found in open literature to date concerning characterisations of dynamic double-directional propagation channels with full azimuth view at both ends of the link. To the best knowledge of the authors, nobody has ever reported the dependency of both DoA and DoD in full azimuth view via extensive experimental investigations. Hence, analysis involving spatial domain properties at both ends of the communication link should be performed in order to provide a more complete treatment of the MIMO directional channel [4].

This paper describes a state-of-the-art wideband dynamic double-directional channel sounding campaign in an outdoor hotspot courtyard environment. The measurements were conducted at 5.2 GHz band (similar to IEEE 802.11a specifications) with a pair of identical 16-element uniform circular patch arrays (UCPAs). The new features of this measurement configuration are threefold. Firstly, the dynamic MIMO responses (16 x 16) along a specific path in the environment can be captured within fine distance-grid steps. This supports dynamic channel modelling activities where the phenomena of dynamic evolution of MPCs along the measurement path can be characterised as a birth/death stochastic process [5] (beyond the scope of this paper). Secondly, the spatial dependency between Tx and Rx, in particular the DoD and DoA in full azimuth view, can be evaluated. It was observed that MPCs tend to concentrate along the axis where both terminals faced each other, where the channel was dominated by MPCs in line-of-sight (LOS) directional region. Thirdly, the MIMO channel capacity can be evaluated realistically from arbitrary antenna array architectures. This is possible since channel responses can be reconstructed based on detailed knowledge of estimated multipath parameters, e.g. DoA, DoD, time delay of arrival (TDoA), and complex path gain [6]. Here, this technique was validated by comparing capacities computed from the reconstructed channel and the real measurement data, where a good agreement has been achieved between both methods.

This paper is organised as follows. Section II describes the measurement procedure in the courtyard environment. Samples of analysed results, e.g. propagation path prediction, joint distributions of multipath parameters, and MIMO capacities, can be found in Section III. Finally, Section IV concludes the paper.

II. Measurement procedure in courtyard environment

The channel sounding campaign was conducted at a carrier frequency of 5.2 GHz using the Medav RUSK MIMO channel sounder [7]. The sounding bandwidth was set to 120 MHz, and the period of the transmitted periodic multitone signal was 1.6 μs. Real time double-directional measurement was conducted using a pair of identical 16-element UCPAs (Figure 1). The UCPAs employed dual-polarisation (horizontal and vertical) circular stacked patch antennas, where the elements were designed using an in-house finite difference time domain (FDTD) tool [8]. Both UCPAs had a radius of 1.28λ (λ denotes carrier wavelength), and the length of the vertical cylindrical ground plane was 6λ. Although the UCPAs were dual-polarised, only vertical polarisation was considered at both arrays throughout the measurements.

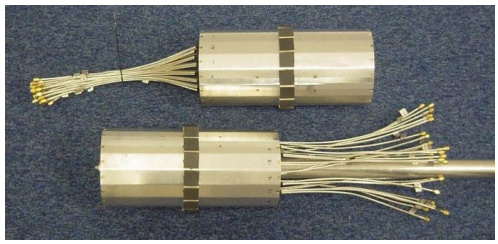

Figure 1: Identical 16-elements dual-polarisation UCPAs

Dynamic measurements were conducted such that the transmitting UCPA was set as the fixed-terminal at a stationary location, while the receiving UCPA was pushed with a customised measurement trolley along a convenient path. The height of the mobile end (Rx) was fixed at 1.7 m at all times (from ground level to the centroid of the patch elements); while the height of the stationary end (Tx) was fixed at either 1.7 m to emulate peer-to-peer link, or 3.0 m to represent an access point (AP). The UCPAs were placed not too close to any local scatterer in order to minimise near-field effect, as spherical wavefront had not been considered in the multipath parameter estimation process. All measurements were conducted in '*time-grid*' mode [7], such that 1 MIMO snapshot (consisted of 16 x 16 complex frequency responses) was recorded every 15.36 ms while the mobile trolley was being pushed at a speed of approximately 0.2 m/s. Channel sounding process was commenced seconds after the trolley was in motion, and was ended just before the trolley reached the final destination point.

In addition, two external 16-port array switching units were constructed in order to provide synchronised sequential switching between all 256 (16 x 16) MIMO channels. Each array switching unit consisted of a pair of 8-to-1 PIN diode switches connected to a single 2-to-1 switch in order to switch between the elements. For the switching unit mounted on the Rx side, the output from the switch was passed through a low noise amplifier (LNA) and bandpass filter before connected to the sounder. In order to isolate as much effect of UCPA circuitry from the propagation channel as possible, the custom-built switching units have been designed in such a way that responses of both LNA and filter were included in back-to-back system calibration process prior to measurements. Also, both switching units were mounted on the UCPAs for array manifold measurements performed in an anechoic chamber, and were not dismounted from the arrays before the total completion of all relevant measurement campaigns. Figure 2 illustrates the MIMO channels synchronised sequential switching sequences at both UCPAs.

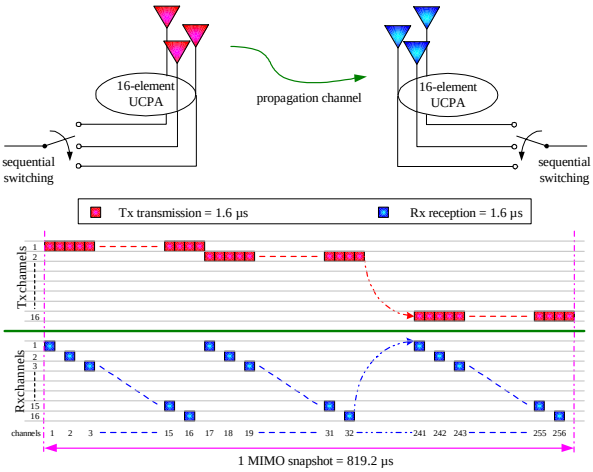

Figure 2: Illustration of MIMO channels switching sequence

The analysis reported in this paper was associated to measurements conducted in an outdoor courtyard environment. The courtyard was an open environment where hotspot wireless communication is likely to take place in future deployment. There were some plants and concrete bricks around the sides of the environment. It should be noted that during the whole measurement process, all efforts have been made to ensure a minimum disruption of the full azimuth view at both ends from any nearby object. The measurement floor plan (reproduced to its nearest geometrical accuracy) and sample pictures of the environment are shown in Figures 3 and 4.

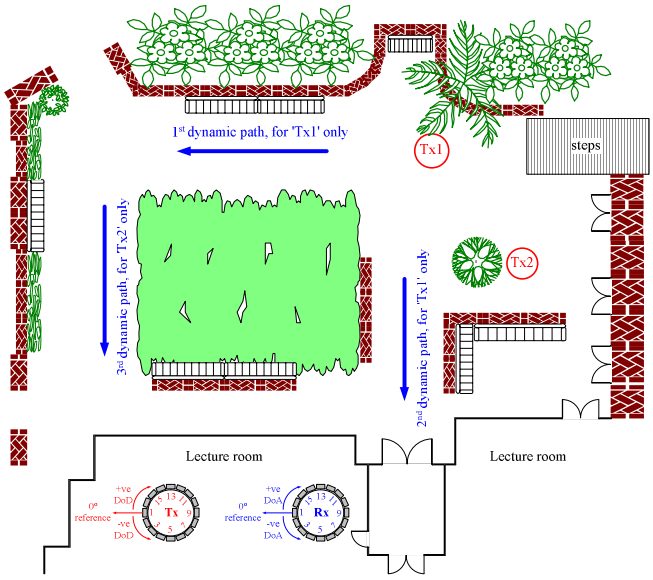

Figure 3: Floor plan of the courtyard environment

a- Tx (3 m in height) at 'Tx1'; Rx (1.7 m in height) along 2nd dynamic path

b- Rx (1.7 m in height) along 3rd dynamic path; Tx (1.7 m in height) at 'Tx2'

Figure 4: Sample pictures in the courtyard environment

III. Samples of Analysed Results

As a precursor to analysing the multidimensional propagation channel, multipath parameters need to be extracted from the measurement data. Here, the 3-D Hybrid-Space Space-Alternating Generalised Expectation-maximisation (HS-SAGE) algorithm [9] was employed to estimate the DoA, DoD and TDoA of the channel. Briefly, the HS-SAGE algorithm was specially developed in order to minimise the resultant complexity and effective processing time of the classical SAGE algorithm. The implementation of the HS-SAGE algorithm was based on the combination of element-space and beamspace processing. For the analysis associated to this paper, the TDoAs were estimated in beamspace domain, while both DoAs and DoDs were estimated in normal element-space domains. In this particular case, complexity reduction and timesaving processing was achieved with the reduction of effective input data size by nearly 50%, as 100 beams (out of 193) were formed in the beamspace domain for the estimation of TDoA within the multidimensional joint estimation problem. Interest reader is referred to [9] for a complete implementation of the HS-SAGE algorithm.

A. *Propagation path prediction*

The propagation paths for the MPCs can be traced based on multidimensional parameters information. Here, it is worth noting that tracing the path propagated by a particular MPC is only possible if its propagation mechanism is not too complex (e.g. without any diffuse scattering), and the environment is not too cluttered. The direction propagated by a particular MPC can be traced back to the scattering objects from both Tx and Rx, providing visualisation of the physical propagation mechanism of the MPC [4]. Single-bounce reflections can be determined with high accuracy and confidence as directional information is

available at both ends, as well as path length knowledge calculated from TDoA. Tracing higher-order reflections is also possible if both directional information and path length match well with the channel (especially the layout and structure of the environment). It should be stressed that although the transmit and receive ends of the double-directional channel have been defined in the measurement campaign, the wireless propagation link is in fact reciprocal. This implies that the radio paths propagated by the MPCs are identical, regardless of whether the radio terminal is a Tx or Rx, i.e. the DoAs are equivalent to DoDs if the Rx is replaced by Tx, and vice-versa. Furthermore, it should be emphasised that the directional gain responses of the arrays have been eliminated when performing computation for the path gain[†], i.e. a total removal of array effects from the propagation channel (assuming ideal condition). The complex path gain represents the strength of the MPC just before impinging on the array, regardless of the nature of propagation mechanism it experiences (e.g. order of reflections, number of interactions with scatterers, additional attenuation caused by transmission, etc).

Here, an example on predicting MPCs propagation paths is given, based on measurement snapshot corresponding to Rx position (along the 3rd dynamic path) at ≈0° direction from the Tx placed at location 'Tx2' (see Figure 3). The height of the Tx in this case was 3 m. The channel condition was considered to be obstructed LOS (OLOS), as the direct LOS path was obstructed by a tree near the Tx. The estimated DoA, DoD, and TDoA results for this particular MIMO snapshot is presented in Figure 5. Based on the results, the MPC propagation paths have been traced in Figure 6, for 10 MPCs most likely to meet accurate prediction. The multipath parameters corresponding to these 10 MPCs are also printed on figure.

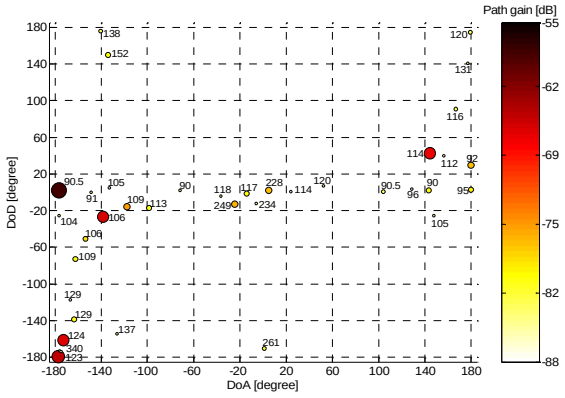

Figure 5: Estimated DoA, DoD, and TDoA results, the path gain is shading-coded and size-coded (bigger size indicates stronger power), and the TDoA value (ns) is printed on figure.

It can be seen that most MPCs with smaller delay (TDoA of <200 ns in general) experienced 1st order reflection, while MPCs with larger delay (TDoA of >200 ns) experienced higher-order reflections. It can also be observed that most MPCs concentrated along the axis where both Tx and Rx faced each other. Due to the structure of the courtyard environment, MPCs with larger delays are expected to exist in the channel. From the estimated result, it can be deduced that 'path 4' and 'path 8' had experienced some sort of interactions with far scatterers located beyond the area of the courtyard environment. Another MPC (labelled as 'path 10') with large delay was predicted to have experienced 3 times of reflections along the axis where both Tx and Rx faced each other. MPCs with apparent large delays are normally modelled as far scatterers [3], and have a role of introducing frequency selectivity into the channel. By knowing the directional regions of the far scatterers, the communication link for applications demanding small delay spread can then be diverted away from these scatterers (by means of smart antenna technologies for example).

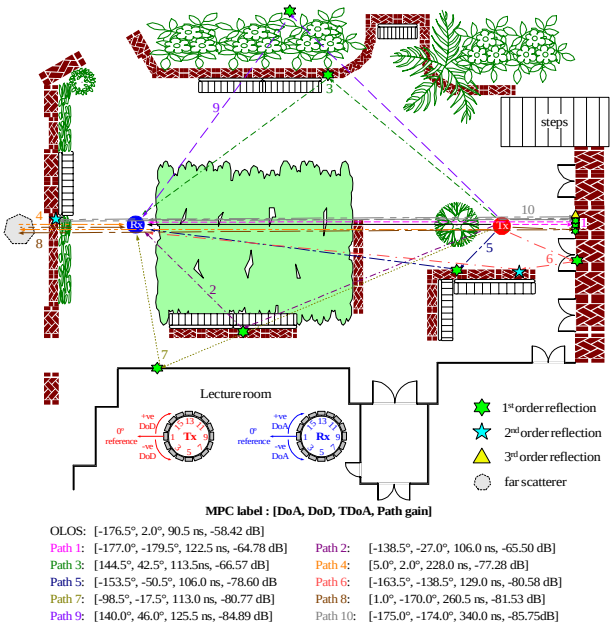

Figure 6: Predicted propagation paths of the MPCs

Moreover, it can be observed that the DoAs and DoDs do not accurately match the geometrical optics in the environment. This was due to the rough and irregularly-shaped surfaces of the objects interacting with the radiowaves that caused additional scattering other than specular reflections (most of the walls and objects surrounding the courtyard environment have rough surfaces). Also, the floor plan of the courtyard had not been reproduced to the exact scale of the environment, as the blueprint for the environment is unavailable. As a final remark, based on the directional knowledge of the channel (i.e. DoA for receiving mode, or DoD for transmitting mode), the deployment of multielement antenna systems should be orientated to face angular regions where significant amount of MPCs tend to concentrate at, in order to ensure a good communication link between the terminals.

B. Joint distributions of multipath parameters

This section presents the joint distributions of the multipath parameters. As the measurements were conducted in dynamic mode, the TDoA and both directional parameters associated to a particular MPC will change as a function of mobile terminal (MT) displacement along the dynamic route. Hence, in order to have a better insight into the overall dependency between the multidimensional parameters, the array orientations were artificially readjusted (in offline processing) such that both UCPAs faced each other at their respective normalised 0° reference axis throughout the whole dynamic path. The TDoAs estimated in each point along the dynamic route were also normalised to the respective 1st arrival path.

Figure 7a presents the joint distributions between the DoA and DoD parameters, for measurements along the 1st and 2nd dynamic paths in which the Tx was placed at location 'Tx1' with a height of 1.7 m – LOS channel condition at all times. The results only display MPCs that have been estimated within a dynamic range of 25 dB relative to the strongest LOS component. It can be seen that MPCs concentrated around the directional regions of normalised 0° at both sides, in particular the LOS direction. Both DoA and DoD parameters were not evenly and independently distributed

[†] It should be noted that the complex path gain of the MPC is not estimated in the HS-SAGE (or SAGE) algorithm, it is however calculated directly from the *complete data* [9] based on the estimated multipath parameters within the estimation process in each iteration.

around the azimuth. When the path gain (power) was taken into consideration, the channel was found to be dominated by MPCs around the LOS directional region, as indicated by the power density shown in Figure 7b. As the measurements employed dual circular arrays capable of providing instantaneous full azimuth view at both ends, the amount of power contributed by weaker MPCs beyond the LOS region became insignificant. In this particular measurement configuration with dual UCPAs, weaker MPCs beyond the LOS region had virtually no power contribution to the channel, as long as power contribution within the LOS region is taken into account. The power azimuth profiles (PAPs) at both sides were found to exhibit Laplacian characteristics with a peak at their respective normalised 0°.

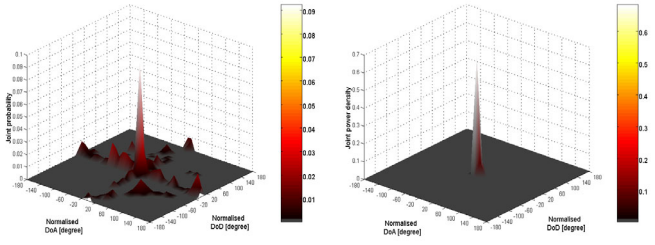

a- 2-D joint distribution b- 2-D joint power density

Figure 7: Joint distribution between DoA and DoD

Both directional parameters were uniformly distributed across the azimuth, with a peak exhibiting Laplacian characteristics around the LOS regions, as shown in Figure 8. The square root of the second central moment of the PDP and PAPs at both sides have been computed, based on MPCs concentrated around the LOS region, i.e. $-50° \leq \phi_{DoA} \leq 50°$ and $-50° \leq \phi_{DoD} \leq 50°$. Figure 9 presents the distributions of these parameters. Due to the LOS condition in the channel, the DoAs, DoDs, and TDoAs have small spreads around the LOS region. Table 1 provides the means and variances of the spread parameters.

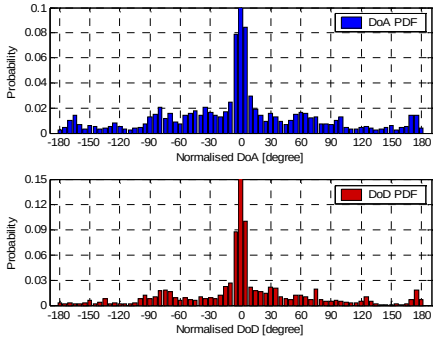

Figure 8: Global distributions of DoA and DoD parameters

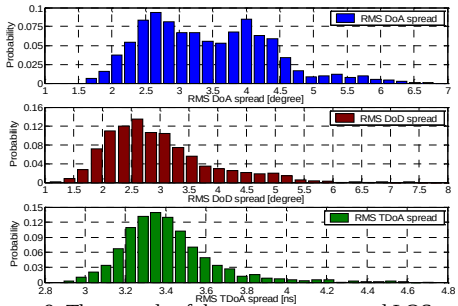

Figure 9: The spreads of the parameters around LOS region

Spread parameters	Mean	Variance
RMS DoA spread	3.41°	0.86°
RMS DoD spread	2.99°	0.99°
RMS TDoA spread	3.41 ns	0.06 ns

Table 1: Means and variances of the spread parameters

The joint distributions between TDoA and both directional parameters are presented in Figure 10. Again, it was found that both TDoA and directional parameters were not independently distributed. It was observed that majority of the MPCs have small excess delays. Within 0-20 ns excess delay range, the propagation of MPCs was confined to LOS directional regions. The amount of MPCs with small excess delays beyond LOS directional regions was relatively more at the Rx compared to that at the Tx. This was due to larger amount of local scatterers around the Rx relative to the Tx. The amount of local scatterers around the mobile Rx was different along the whole dynamic path; whereas the number of local scatterers was considered constant around the stationary Tx throughout the measurements. Further, it can also be observed that MPCs with larger delays concentrated along the LOS directional axis. As shown in the example of propagation path prediction in Figure 6, these MPCs have undergone multiple reflections and interactions with far scatterers. Clustering phenomena can also be observed, where the cluster with largest amount of MPCs was due to MPCs with small excess delay propagated along the LOS directional axis.

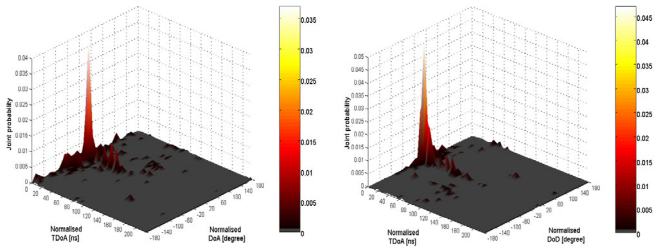

a- TDoA and DoA b- TDoA and DoD

Figure 10: 2-D joint distribution of TDoA and DoA/DoD parameters

C. *Capacity of MIMO channels*

It is well known that MIMO systems can offer significant improvement in terms of spectral efficiency [10], such that the channel capacity increases linearly with the number of transmit and receive antennas (assuming a same number of elements at both sides). The natures of channel propagation conditions and antennas employed in the system form an influential factor in determining the ultimate capacity of the channel [11]. Due to various difficulties in performing full scale MIMO measurements with different antenna array architectures, channel capacity calculated from synthetic channel responses based on estimated multipath parameters has been proposed in [6].

This section provides validation on the capacity computation technique proposed in [6], whereby MIMO channel responses are reconstructed based on the knowledge of multipath parameters and desired array architecture. Different realisations of MIMO responses are generated by assigning random phase (uniformly distributed) to the complex path gain of the MPCs. Here, the MIMO capacities have been evaluated based on 2 different 4 x 4 subarray configurations (refer to Figure 3 for elements index):

1st configuration - elements 1-3 and 16 at both sides

2nd configuration - elements 4-7 at Tx, and elements 12-15 at Rx

The transmit power was assumed to be equally distributed over the 4 Tx antennas, with signal-to-noise ratio (SNR) of 20 dB, and the channel responses were normalised to the channel coefficients that experienced the lowest mean pathlosses as seen by each port of the subarrays [12]. Based on this, the channel capacities were computed from measurement data and synthetic data for comparison. For the synthetic case, a total of 100 realisations were generated based on '*random phase assignment*' [6] for each of the estimated parameter results associated to each location of the mobile Rx along the dynamic path.

Figure 11 presents the distributions of normalised capacities calculated from narrowband (flat fading case) and wideband (120 MHz bandwidth, frequency selective case) channels, with the 1st subarray configuration, for measurements associated to 'Tx1' and 2nd dynamic path. It can be seen that distributions of capacity computed from both methods are virtually identical, demonstrating an excellent agreement between both methods. As expected, the distribution for the wideband case has a lower variance, due to additional diversity caused by frequency selectivity. Also, the instantaneous capacity (averaged across 100 '*random phase*' realisations and 120 MHz bandwidth) computed from synthetic data along the whole dynamic path also matched well with that computed from real measurement data, as shown in Figure 12.

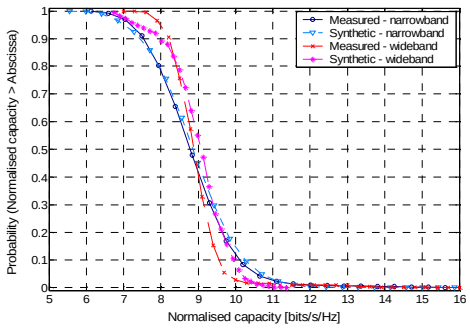

Figure 11: Distributions of capacity for 1st subarray configuration

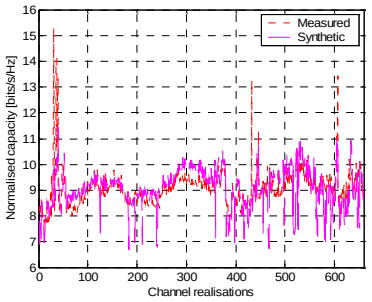

Figure 12: Instantaneous capacity (wideband channel) across the whole 2nd dynamic path, for the 1st subarray configuration

However, in some instances where the synthetic data underestimates the capacity due to 'unaccounted MPCs' in the multipath parameter estimation process, random Gaussian noise should be added to the resultant synthetic response in order to provide further decorrelation to the channels (further details in [6]). This is shown in Figure 13 for the case of 2nd subarray configuration, where the normalised capacity was underestimated by 0.665 bits/s/Hz on average (nevertheless the result in this case was considered reasonably good). In this particular case, random Gaussian noise of -25 dB (noise power) relative to the coefficient with highest path gain was added to the synthetic channel. As a result, the capacities computed from both measured and synthetic data were found to exhibit an excellent match between them. Hence, capacity of MIMO channels based on arbitrary antenna arrays and elements designs, with different orientations across the azimuth from both sides, can be evaluated in a realistic manner without the need of performing additional measurement campaigns with new arrays and settings.

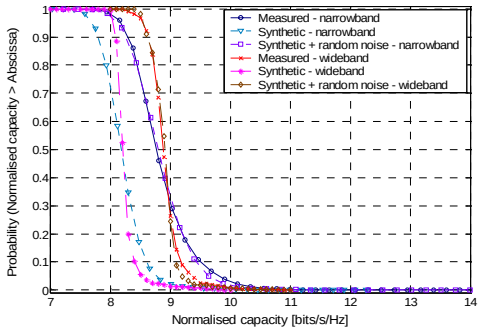

Figure 13: Distributions of capacity for 2nd subarray configuration

IV. Conclusions

This paper has described the state-of-the-art wideband dynamic double-directional channel sounding campaign in an outdoor courtyard environment at 5.2 GHz. The measurement employed a pair of identical 16-element UCPAs in order to provide instantaneous full azimuth view of the channels at both ends. Analysed results revealed that both DoA and DoD were not independently and evenly distributed across the azimuth, where both parameters were found to concentrate along the LOS axis. In addition, the MIMO capacity evaluated from the synthetic channel constructed from estimated multipath parameters was found to match well with that computed from real measurement data.

Acknowledgements

The authors would like to thank Dr. Dominique Paul and Mr. Ken Steven for the design and construction of the UCPAs, as well as Ofcom for the financial support of this measurement campaign.

References

[1] J. H. Winters, "Smart antenna for wireless systems," IEEE Personal Communications, February 1998, pp. 23-27.

[2] M. Chryssomallis, "Smart antennas," IEEE Antennas and Propagation Magazine, vol. 42, no. 3, June 2000, pp. 129-136.

[3] L. M. Correia (ed.), Wireless Flexible Personalised Communications, COST 259: European Co-operation in Mobile Radio Research, New York, Wiley, 2001.

[4] M. Steinbauer, A. F. Molisch, and E. Bonek, "The double-directional radio channel," IEEE Antennas and Propagation magazine, vol. 43, no. 4, August 2001.

[5] C. C. Chong, D. I. Laurenson, C. M. Tan, S. McLaughlin, M. A. Beach and A. R. Nix, "Modelling the dynamic evolution of paths of the wideband indoor propagation channels using the M-step, 4-state Markov model," 5th EPMCC, Glasgow, Scotland, U.K., 22-25 April 2003.

[6] A. F. Molisch, M. Steinbauer, M. Toeltsch, E. Bonek, R. S. Thomä, "Capacity of MIMO systems based on measured wireless channels," IEEE JSAC, vol. 20, no. 3, April 2002, pp. 561-569.

[7] http://www.medav.de, dated 22 June 2004.

[8] D. L. Paul, I. J. Craddock, C. J. Railton, P. N. Fletcher, and M. Dean, "FDTD analysis and design of probe-fed dual-polarised circular stacked patch antenna," Microwave and Optical Technology Letters, vol. 29, May 2001, pp. 223-226.

[9] C. M. Tan, M. A. Beach, and A. R. Nix, "Multidimensional hybrid-space SAGE algorithm: Joint element-space and beamspace processing," IST Mobile and Wireless Communications Summit 2003, Aveiro, Portugal, 15-18 June 2003.

[10] G. J. Foschini, and M. J. Gans, "On the limits of wireless communications in fading environments when using multiple antennas," Wireless Personal Communications, vol. 6, 1998, pp. 311-335.

[11] M. Beach, M. Hunukumbure, C. Williams, G. Hilton, P. Rogers, M. Capstick, and B. Kemp, "An experimental evaluation of three candidate MIMO array designs for PDA devices," European COST 273/284 Joint Workshop, Gothenburg, Sweden, 7-10 June 2004.

[12] D. P. McNamara, "Characterisation and investigation of multiple-input multiple-output wireless communication channels," Ph.D. Thesis, University of Bristol, U.K., March 2003.